Quantification of Myocardial Blood Flow Using Dynamic Nitrogen-13-Ammonia PET Studies and Factor Analysis of Dynamic Structures

Hsiao-Ming Wu, Carl K. Hoh, Denis B. Buxton, William G. Kuhle, Heinrich R. Schelbert, Yong Choi, Randall A. Hawkins, Michael E. Phelps and Sung-Cheng Huang

Division of Nuclear Medicine and Biophysics, Department of Molecular and Medical Pharmacology, Laboratory of Structural Biology and Molecular Medicine, UCLA School of Medicine, Los Angeles, California

In this study, factor analysis of dynamic structures (FADS) was used to extract the "pure" blood-pool time-activity curves (TACs) and to generate parametric myocardial blood flow (MBF) images (pixel unit: ml/min/g). **Methods:** Ten dynamic ^{13}N-ammonia dog PET studies (three baseline, five hyperemia and two occlusion) were included. Three factors (TACs) and their corresponding factor images (the right ventricular and left ventricular blood pools and myocardial activities) were extracted from each study. The left ventricular factors matched well with the plasma TACs. The factor images of myocardium were then converted to a parametric images of MBF using a relationship derived from a two-compartment model. **Results:** MBF estimates obtained from FADS correlated well with MBF estimates obtained with the two-compartment model ($r = 0.98$, slope = 0.84) and microsphere techniques ($r = 0.96$, slope = 0.94). FADS-generated MBF parametric images have better image quality and lower noise levels compared to those generated with Patlak graphical analysis. **Conclusion:** Regional MBF can be measured accurately and noninvasively with ^{13}N-ammonia dynamic PET imaging and FADS. The method is simple, accurate and produces parametric images of MBF without requiring blood sampling and spillover correction.

Key Words: factor analysis; positron emission tomography; parametric image

J Nucl Med 1995; 36:2087–2093

Dynamic ^{13}N-ammonia PET imaging, together with a two-compartment tracer kinetics model, permits the noninvasive quantification of regional myocardial blood flow in both human studies and canines (*1–3*). Kuhle et al. demonstrated that calculated regional values of MBF (ml/min/g) obtained with the two compartment dynamic ^{13}N-ammonia PET method correlated well with values obtained from the microsphere technique (*3*). The standard modeling approach requires blood sampling to measure the input function and time-consuming nonlinear regression on each regional myocardial time-activity curve (TAC). Without spillover correction, the bi-directional cross-contamination of activities (between blood pool and myocardium) in PET images may affect the accuracy of MBF estimates (*4*). We demonstrated the feasibility of factor analysis of dynamic structures (FADS) to accurately extract the "pure" blood TAC directly from dynamic ^{13}N-ammonia PET images in a previous study (*5*). This technique makes it possible to generate quantitative estimates and parametric images of MBF with ^{13}N-ammonia PET dynamic studies without blood samples, region of interest (ROI) definition or spillover corrections.

FADS has previously been used to decompose dynamic sequences in component images and their corresponding TACs in nuclear medicine (*6–11*). The technique is based on principal component analysis followed by oblique rotations with positivity constraints (*10*). The algorithm assumes that a dixel (defined as the pixel activity as a function of time) of a dynamic study is a linear combination of a small number of fundamental TACs termed physiological factors. Each physiological factor is associated with an independent physiological structure (e.g., ventricular cavity blood pool). Although the factors can be numerically determined from FADS, considerable error can be found if the component structures are physically overlapped by one another (*12*). In tomographic images such as PET images, although different anatomical structures are spatially separated, the partial volume effects and activity spillover problems may cause the activity in one structure to be contaminated with activity from an adjacent structure.

In this study, the potential utility of FADS generated factors and factor images to quantitate and map MBF was studied using ten dynamic ^{13}N-ammonia PET canine studies. The relationship between MBF and myocardial pixel value in myocardial factor images was derived based on the two-compartment ^{13}N-ammonia MBF model. This eliminated the time-consuming nonlinear regression step for each regional MBF calculation, and the results were used to convert myocardial factor images into parametric images of MBF. FADS-generated MBF parametric images were com-

Received Nov. 23, 1994; revision accepted Apr. 12, 1995.

For correspondence or reprints contact: Carl K. Hoh, MD, Division of Nuclear Medicine and Biophysics, Department of Molecular and Medical Pharmacology, UCLA School of Medicine, 10833 Le Conte Avenue, Los Angeles, CA 90095-6948.

pared to MBF parametric images generated by a method based on Patlak graphical analysis previously developed in our laboratory (*13*). The numerical accuracy of MBF estimates obtained with FADS was evaluated by comparing the results to those obtained with the microsphere technique and the standard two-compartment tracer kinetic model.

MATERIALS AND METHODS

Nitrogen-13-Ammonia Dog PET Studies

Ten dynamic ^{13}N-ammonia PET studies (three baseline, five dipyridamole induced hyperemia and two coronary occlusion) from a previous study conducted in our laboratory were used (*3*). These PET studies were performed in four mongrel dogs (weighing 25 to 32.5 kg). Following intravenous injection of ^{13}N-ammonia (20 mCi in 2–8 ml saline), dynamic images were obtained with a tomograph. The dynamic sequence consisted of twelve 10 sec and six 20 sec scans for a total scan time of 4 min. Four gated frames, equally gated based on the electrocardiographic lead II signal, were acquired immediately after the dynamic sequence for 20 min.

Blood samples were taken from the abdominal aorta at 10 sec interval for the first 2 min. In addition, four blood samples were taken at 40, 80, 120 and 180 sec to determine the nonammonia metabolites in the arterial input function. Assays of ^{13}N plasma concentrations were performed in a well counter after centrifugation of the blood samples. The percentages of nonammonia metabolites in the blood at the times between the samples were derived by linear interpolation of metabolites determined from the four arterial samples. Each blood TAC was corrected for physical decay and nonammonia metabolites. A cylinder phantom filled with ^{68}Ge/^{68}Ga solution was scanned on the same day of the PET study to determine the conversion factor between image data in units of counts per minute per pixel and well counter data in units of counts per minute per milliliter.

The 128 × 128 (1.38 mm^2/pixel) transaxial images were reconstructed using a Shepp-Logan filter with a cutoff frequency of 0.48 Nyquist frequency, yielding an in-plane spatial resolution of ~10.5 mm FWHM. Fifteen simultaneous cross-sectional images, with 6.75 mm plane separation, were generated with a total axial field of view of 10.8 cm. Photon attenuation was corrected with a 20-min transmission scan using a ^{68}Ge/^{68}Ga external ring source. The 15 contiguous transaxial images of each study were then reoriented into 6 left ventricular short-axis slices as previously described (*14*). In each study, the diastolic frames of gated study and ungated dynamic frames were reoriented into short-axis images using the same reorientation parameters.

Microsphere Studies

Regional MBF for each study was measured independently with radioactive carbonized polystyrene microspheres (15 μ). Simultaneous with the intravenous injection of ^{13}N-ammonia, approximately 2 × 10^6 microspheres labeled with scandium-46, niobium-95, tin-113, or ruthenium-103 were injected over 15 sec into the left atrium. Arterial blood was withdrawn at a constant rate of 7.2 ml/min for 2 min and counted in a well counter for microsphere activity. After completion of the studies, the heart was removed, washed and cut into 1-cm thick left ventricular short-axis cross sections. After each section had been photographed, it was subdivided further into 0.5- to 1-g tissue samples, each of which was counted in a well counter for its microsphere activity concentration. Regional MBF by microspheres (ml/min/g) was then calculated (*15*).

Estimation of Regional MBF Using a Two-Compartment Model

For regional MBF estimation, each short-axis myocardial section (midventricular plane, either plane 2 or 3 of 6 contiguous short-axis planes) was divided into eight sectors (10 dog studies, 80 sectors in total). The eight (45° for each sector) sectorial region of interests were defined by the two contours separated radially by three pixels (1.17 mm/pixel) and centered at the peak of myocardial circumferential activity (*3*). In the model fitting, the 45° sectors were first defined using the last frame of the dynamic sequence (pixel unit: counts/sec). The eight sectorial TACs were then derived by applying the same sectors to the entire dynamic sequence. Sectorial recovery coefficients for a given image were obtained by profile analysis of the activity across the myocardial wall on the diastolic gated image (*3,16*). For each study, short-axis image reorientation (*14*), myocardial sector structure and recovery coefficient determination (*3,16*) were processed using an image processing program EXPLORER (UCLA) implemented in a Macintosh® II computer.

The two-compartment model established by Smith et al. and validated by Kuhle et al. was used for estimating regional MBF (ml/min/g) (*1–3*). The initial 2 min of kinetic data were used for analysis. The model contains a freely diffusible ^{13}N-ammonia compartment and a second compartment containing metabolically trapped ^{13}N label (*2*). K_1 (ml/min/g) and k_2 (min^{-1}) represent the forward and reverse rates for exchange between these two compartments. The term V (ml/g) represents the physical distribution volume of free ^{13}N-ammonia in myocardium. At any time t after injection, total ^{13}N activity in the myocardial ROI (Qi(t), cpm/pixel) is the sum of the radioactivity in the free diffusible ($Q_1(t)$, cpm/pixel) and in the trapped ($Q_2(t)$, cpm/pixel) compartments. Spillover (SP_{bt}) from blood-pool activity (AB(t), cpm/pixel) to myocardium activity is also included. Therefore,

$$Q_i(t) = Q_1(t) + Q_2(t) + SP_{bt} \cdot AB(t). \qquad \text{Eq. 1}$$

The radioactivity change rate in the freely diffusible ($dQ_1(t)/dt$) and trapped ($dQ_2(t)/dt$) compartments in myocardium can be described by the following equations:

$$\frac{dQ_1(t)}{dt} = -\frac{K_1 + MBF}{V} Q_1(t) + k_2 Q_2(t) + MBF \cdot C_a(t) \qquad \text{Eq. 2}$$

$$\frac{dQ_2(t)}{dt} = \frac{K_1}{V} Q_1(t) - k_2 Q_2(t), \qquad \text{Eq. 3}$$

where $C_a(t)$ is the arterial input function. Replacement of tissue blood radioactivity ($C_a(t)$) with plasma radioactivity was validated by Weinberg et al. (*17*). In this model, V was fixed at 0.8 ml/g and k_2 was set to 0 during the first 2 min after tracer injection because of the relatively long clearance half-times of trapped ^{13}N activity (*1*). The model is relatively insensitive to errors in k_2 and V, as previously shown by Krivokapich et al. (*2*). Furthermore, the relationship between K_1 and MBF (*18*),

$$K_1 = MBF[1.65e^{(1.25/MBF)} - 1], \qquad \text{Eq. 4}$$

was used during model fitting to reduce the number of variable parameters to two parameters, MBF and SP_{bt}. This model has been validated in canine studies (*3*). A good relationship between MBF and the rate-pressure product in human studies at rest also supports the approximation used in this model (*19*).

Generation of Parametric MBF Image Using Patlak Graphical Analysis

The dynamic frames obtained from 70 to 120 sec after ^{13}N-ammonia injection and plasma TAC were used to generate the Patlak parametric MBF images using the method described by Choi et al. (*13*). The following Patlak equation was evaluated on a pixel-by-pixel basis:

$$\frac{Q_i(t)}{C_a(t)} = K\frac{\int_0^t C_a(\tau)\,d\tau}{C_a(t)} + \frac{MBF^2V}{(MBF + K_1)^2} + SP_{bt}\frac{AB(t)}{C_a(t)}, \qquad \text{Eq. 5}$$

where K, the slope of the straight portion of the Patlak plot (normalized counts, $Q_i(t)/C_a(t)$, versus normalized time, $\int_0^t C_a(\tau)\,d\tau/C_a(t)$), is related to the MBF by the following equation:

$$K = MBF[1 - 0.607e^{-(1.25/MBF)}]. \qquad \text{Eq. 6}$$

Since a better correlation was found between the constrained Patlak graphical analysis and the two-compartment model results (*13*), the parametric images were generated by constraining the intercept ($MBF^2V/(MBF + K_1)^2 + SP_{bt} \cdot AB(t)/C_a(t)$) of the Patlak equation within the physiologically acceptable range (lower limit: 0.43, upper limit: 0.65) suggested by Choi et al. (*13*).

FADS of Ungated Dynamic Images

This study used the FADS algorithm originally established by Barber and Di Paola et al. (*6,10*). The method generates physiological factors and factor images using normalized TACs from each dixel. Each dixel, treated as an n-dimensional vector (n = total frame number of dynamic study), was assumed to be a linear combination of the "pure" physiologic TACs. Using principal component analysis of the dixels, a new reference vector space was created which could be iteratively rotated until all factors and factor images were positive. In summary, four steps were involved in this algorithm: (a) data preprocessing; (b) principal component analysis; (c) oblique rotation under positivity constraints; and (d) factor image computation. Two modifications were used in the present study. First, we found that weighting the normalized dixel vectors to scan duration improved the accuracy of the algorithm. Second, we computed the coordinates of the oblique factors by minimizing the negative values in both the factors and the factor images using a constrained optimization routine (MATLAB®, MathWorks, Inc. Natick, MA). This latter modification resulted in a faster convergence speed.

Figure 1 is the flowchart for the FADS MBF calculation used in this study. The 128 × 128 × 18 short-axis dynamic images (the same image plane used in the two-compartment model fitting) were first masked to form a 64 × 64 × 18 dynamic image file. The masked area includes right and left ventricular blood pools and the entire myocardium. The masked images were then submitted to the FADS algorithm. The first three factors were extracted, accounting for ~95% of the total variance in the data. The three 64 × 64 factor images were then computed by projecting all the dixels of the original masked 64 × 64 dynamic images on the three factors. To be consistent with the two-compartment model fitting and Patlak graphical analysis, only the initial 2-min kinetic data were used to generate the factor images.

Estimation of Regional MBF and Generation of Parametric MBF Images Using FADS

Integration of Equations 2 and 3, assuming k_2 is negligible, results in:

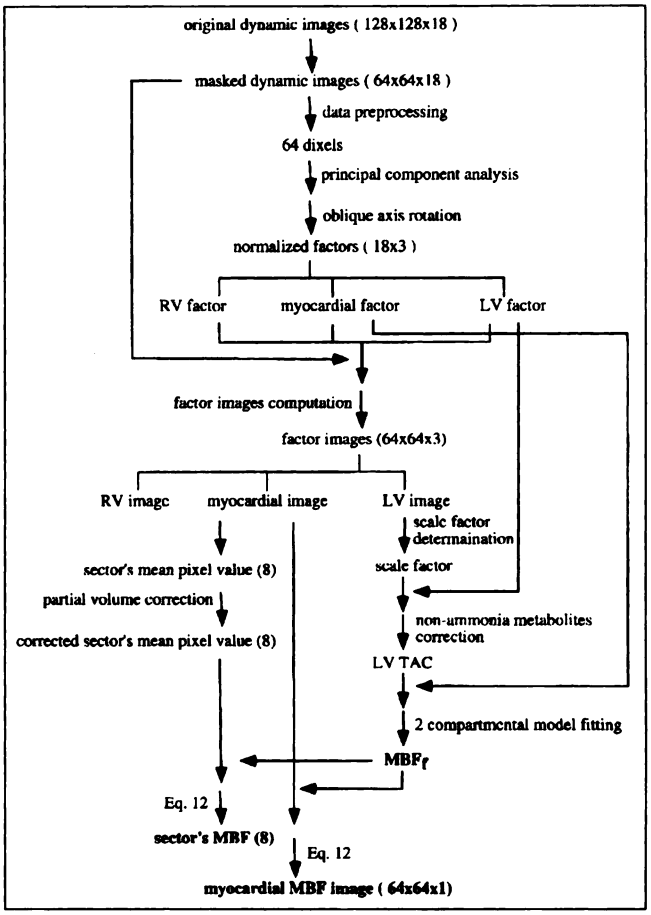

FIGURE 1. Flowchart of FADS algorithm and MBF calculation used in all 10 dog studies.

$$Q_1(t) = -\frac{K_1 + MBF}{V}\int_0^t Q_1(\tau)\,d\tau + MBF\int_0^t C_a(\tau)\,d\tau. \qquad \text{Eq. 7}$$

$$Q_2(t) = \frac{K_1}{V}\int_0^t Q_1(\tau)\,d\tau. \qquad \text{Eq. 8}$$

Since FADS can separate blood-pool activity from myocardial activity, the SP_{bt} term in Equation 1 can be ignored. By substituting $Q_1(t)$ and $Q_2(t)$ in Equation 1, assuming SP_{bt} is negligible and using the relationship that $Q_1(t) = MBF \cdot V(K_1 + MBF)^{-1} \cdot Ca(t)$ at equilibrium (when at $t \geq t_\infty$, $dQ_1(t)/d(t) = 0$ in Eq. 2) (*13*), the following equation is obtained:

$$Q_i(t) = \frac{K_1MBF}{K_1 + MBF}\int_0^t C_a(\tau)\,d\tau + \frac{MBF^2V}{(MBF + K_1)^2}C_a(t). \qquad \text{Eq. 9}$$

On the right side of Equation 9, the second term, $MBF^2V/(MBF + K_1)^2 \cdot C_a(t)$, is negligibly small compared to the first term, $((K_1MBF)/(K_1 + MBF) \cdot \int_0^t C_a(\tau)\,d\tau$. For example, when at $t \geq 1$ min, ≤4% if MBF is smaller than 5 ml/min/g; ≤0.3% if MBF is smaller than 0.5 ml/min/g) and can thus be ignored. Further support for the omission of the second term will be shown by results in Figure 6. Therefore, by omitting the second term and substituting K_1 in Equation 9 using Equation 4, one has:

$$Q_i(t) = MBF[1 - 0.607e^{(-1.25/MBF)}] \int_0^t C_a(\tau)\, d\tau. \quad \text{Eq. 10}$$

Let $Q_f(t)$ be the myocardial factor and MBF_f be the MBF estimate of the myocardial factor using two-compartment model fitting, thus:

$$\frac{Q_i(t)}{Q_f(t)} = \frac{MBF[1 - 0.607e^{(-1.25/MBF)}]}{MBF_f[1 - 0.607e^{(-1.25/MBF_f)}]}. \quad \text{Eq. 11}$$

If MBF_f is small (e.g. <0.3), $[1 - 0.607e^{(-1.25/MBF_f)}]$ will approximate 1.0 and the MBF of a region i can be calculated using the following relationship:

$$\frac{Q_i(t)}{Q_f(t)} \times MBF_f = MBF[1 - 0.607e^{(-1.25/MBF)}], \quad \text{Eq. 12}$$

where $Q_i(t)/Q_f(t)$ is the pixel value of the myocardial factor image at region i. In this study, the MBF_f was estimated using the FADS-generated left ventricular TAC and myocardium factor fitted to the two-compartment model. We validated the extraction of left ventricular TAC using FADS and ^{13}N-ammonia dog PET studies in a previous study (*5*). The FADS-generated left ventricular TACs matched the arterialized well counter measurements (see Fig. 7). When MBF_f was larger than 0.3, it was adjusted to a smaller value by dividing the myocardial factor with a scale factor (greater than 1.0) before model fitting and multiplying the myocardial factor image with the same scale factor. The parametric MBF image was then generated from the myocardial factor image using the relationship of Equation 12 on a pixel-by-pixel basis.

For regional MBF estimation, the eight mean sectorial MBF values were obtained by defining the 45° sectors in the myocardial factor image (pixel unit: ml/min/g). Since the counts in the original dynamic images were directly related to the MBF values in the myocardial factor image, the eight 45° sectors delineated in the factor images were very similar to those delineated in the original dynamic images. Partial volume effects were corrected using sectorial recovery coefficients obtained from the diastolic gated image (*3*). Due to the rapid serial image phase of the study protocol, only the ungated dynamic images were acquired. Ideally, the TACs derived from the ungated images should be corrected for partial volume effects and cardiac motion. Activity recovery based solely on the diastolic activity thickness, however, was used due to:

1. The heart spends a greater fraction of the cardiac cycle in diastole. The ungated images therefore have more of a diastolic character.
2. The activity-smearing effects of heart motion offset the underestimation of true myocardial activity using recovery coefficients derived from the diastolic images (*3*).

The sectorial MBFs were then calculated using the mean pixel value of each sector and Equation 12 (Fig. 1) by a table-lookup approach.

RESULTS

Figures 2 and 3A show the three factor images and three FADS-generated factors in a ^{13}N-ammonia dog PET study. The results were consistent in all ten dog studies. The three factors were similar to the TACs generated from ROI (right ventricular: ~170 mm^2; left ventricular: ~390 mm^2 and myocardium: ~20 mm^2) drawings on three structures in the original dynamic images (Fig. 3B). The ROIs were carefully defined to minimize spillover. Bi-directional cross-contamination (spillover) of activities were not observed in the left ventricular and myocardial factors. That is, the left ventricular factor decreased monotonically and no late increase in left ventricular factor values resulting from activity spillover from tissue to the left ventricular cavity was observed. Additionally, no early "vascular peak" was evident in the myocardial factors.

Figure 4 includes selected images from ten studies at a

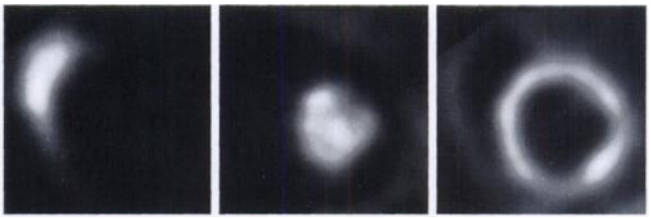

FIGURE 2. Three factor images obtained from a dynamic ^{13}N-ammonia dog PET study from FADS. Structures were identified as (left) right ventricular, (middle) left ventricular blood pools and (right) myocardium. Results were consistent in all 10 studies.

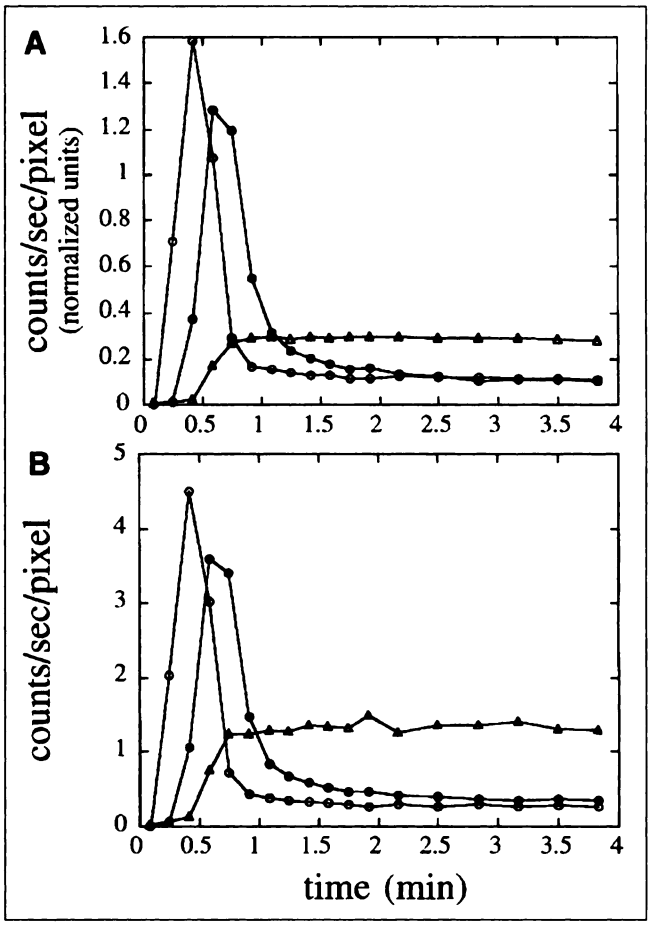

FIGURE 3. (A) Three factors obtained from a dynamic ^{13}N-ammonia dog PET study from FADS. Each factor corresponded to right ventricular (open circle), left ventricular (solid circle) blood pools or myocardial activities (open triangle). (B) ROI-generated TACs from the original dynamic images of the same dog. Results were consistent in all ten studies.

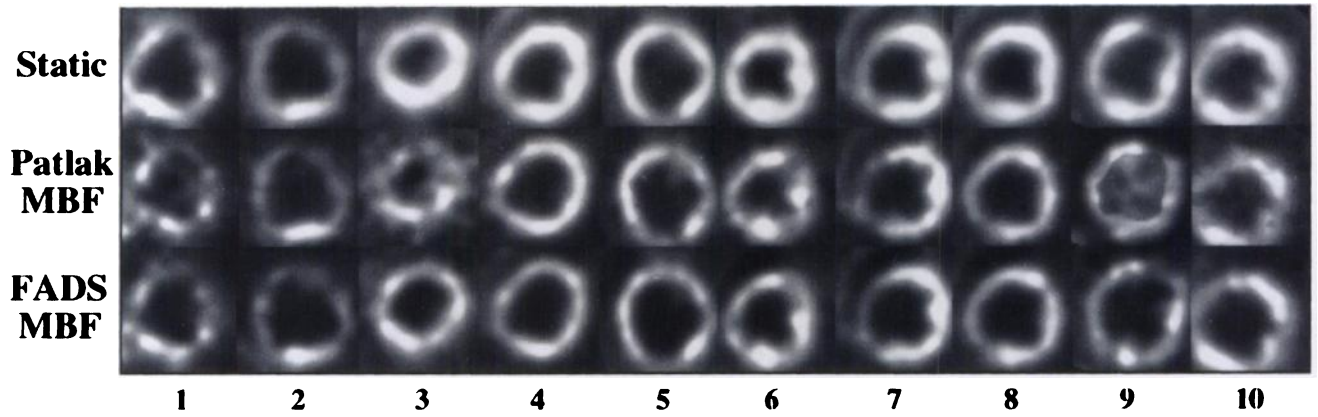

FIGURE 4. Activity distributions (cps/pixel) and parametric MBF images (pixel unit: ml/min/g) from ten dynamic ^{13}N-ammonia dog PET studies. From left to right: baseline studies (images 3, 6, 10); hyperemia studies (images 1, 2, 4, 7, 8); occlusion studies (images 5, 9). (Row 1) Image activity distributions accumulated 3 to 4 min after ^{13}N-ammonia injection. (Row 2) Parametric MBF images using Patlak graphical analysis. (Row 3) Parametric MBF images from FADS and Equation 12.

single image plane. Images in the first row are activity distributions accumulated 3 to 4 min after ^{13}N-ammonia injection. Images in the second row are the MBF parametric images using Patlak graphical analysis, while images in the third row are FADS MBF parametric images. Compared to the activity distribution images (row 1), the factor images (row 3) had lower noise levels. In addition, the spillover activities from the left ventricular chamber to myocardium could be taken into account by the factor analysis. Although Patlak parametric images had increased contrast between the myocardial and background tissues (comparing rows 1 and 2 images), the y-intercept constraint in Patlak analysis can introduce artifacts in the image (e.g., ninth image in row 2). Notice that the parametric images generated by FADS have lower noise levels compared with Patlak parametric images (comparing row 2 and row 3 images).

Figure 5A shows the correlation of sectorial myocardial blood flows obtained from the FADS and microsphere study in ten dog studies. Good correlation, r equals to 0.96, was obtained ($y = 0.94x + 0.09$, $r = 0.96$, $n = 80$). Figure 5B shows the correlation of sectorial MBFs obtained from FADS and the two-compartment model methods ($y = 0.84x + 0.20$, $r = 0.98$, $n = 80$). Whereas the two-compartment model required blood sampling and nonlinear regression for each sectorial TAC (eight sectors per myocardium), FADS requires only one nonlinear regression to the FADS myocardial factor. When the pure sectorial TACs were generated by multiplying the myocardial factor by the mean sectorial pixel values of the factor image and fitted using the two-compartment model, the correlation of MBFs from model fitting and FADS improved and approximated 1 (Fig. 6). The results validated the assumptions used in the derivation of Equation 12.

DISCUSSION

This study demonstrates that FADS technique together with a relationship (Eq. 12) derived from two-compartment modeling provides a simple method for generating MBF parametric images using dynamic ^{13}N-ammonia PET studies. The FADS method is advantageous in that blood sampling, ROI definition, spillover corrections and nonlinear regression on each regional TAC are not required. Furthermore, FADS can compress the entire dynamic PET studies into a limited number of factors and factor images (e.g., three factors and three factor images in this study). Regional MBFs from the FADS technique correlated well with those obtained with the two-compartment model and the microsphere technique ($r = 0.98$ and 0.96, respectively).

There are limitations in FADS:

1. Each component structure should be homogeneous (i.e., all points in the myocardial structure can be described by the same model function and are different only in the magnitude).
2. FADS can separate structures only if there is an incomplete overlap. The requirement that the entire myocardium is homogeneous may not be exactly valid, but it is approximately true over the MBF range of 0.5 ~ 3.5 ml/min/g.

In PET imaging, in which the final resolution is about 10 mm (FWHM), although different anatomical structures (e.g., myocardium and left ventricular blood pool) are spatially separated, partial volume effects and spillover problems may cause activity in one structure to be contaminated with activity from an adjacent structure. If the blood pool and myocardial activities are mostly overlapped in the dynamic images, there will be cross-contamination between the FADS factors. Figure 7 shows the plasma samples corrected for nonammonia metabolites and the FADS-generated left ventricular factor (also after metabolites correction) from a dog study. Except for a time lag of the plasma samples, the overall shapes of plasma samples and left ventricular factor were similar, the spillover activity from the myocardial was negligible (e.g. lack of a high tail of left ventricular factor). The time lag of the plasma sam-

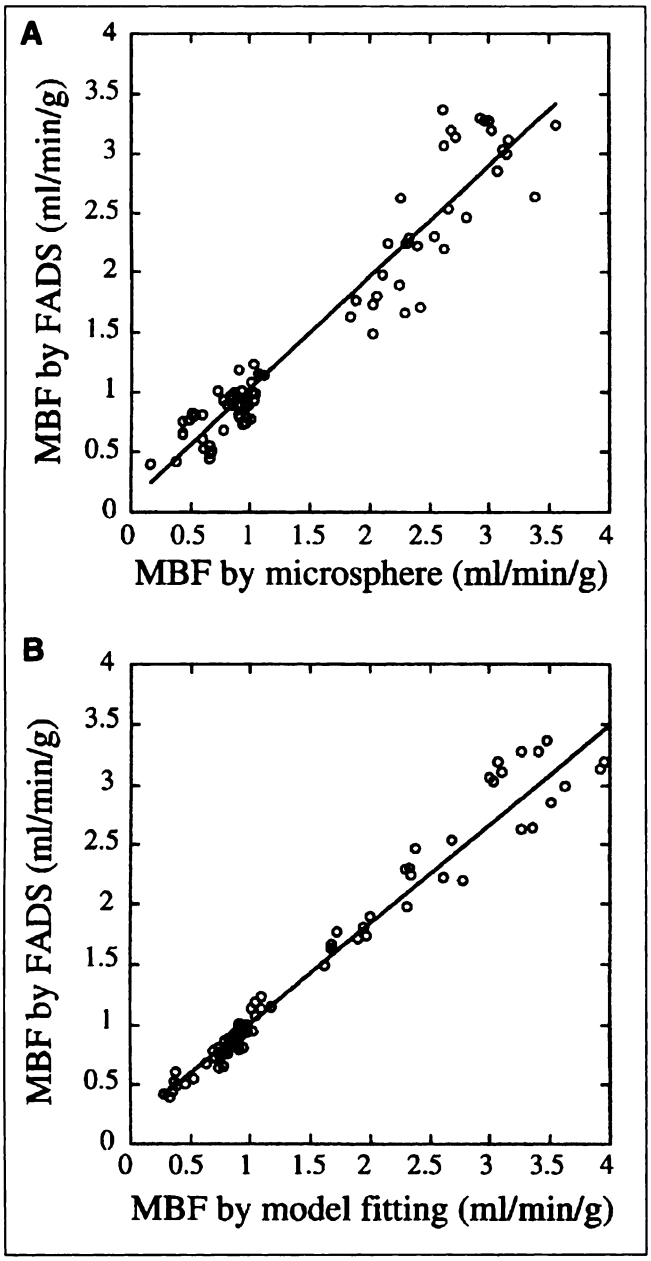

FIGURE 5. Correlation of sectorial MBFs obtained from (A) FADS and the microsphere technique (y = 0.94x + 0.09, r = 0.96, n = 80) and (B) FADS and conventional two-compartment model fitting (y = 0.84x + 0.20, r = 0.98, n = 80).

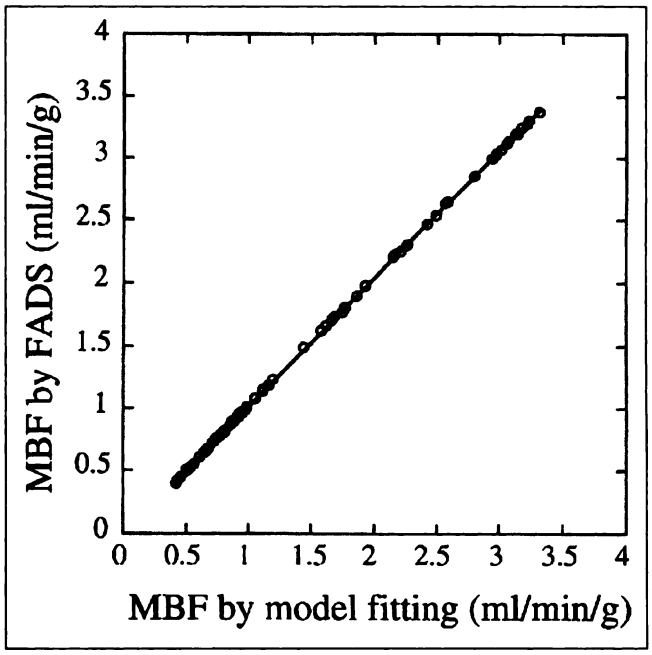

FIGURE 6. Correlation of sectorial MBFs obtained from FADS and conventional two-compartment model fitting (y = 1.03x − 0.01, r = 1.0, n = 80). Sectorial TACs in two-compartment model fitting used pure TACs obtained by subtracting blood-pool spillover activity from the original TACs (which is equals to the mean sectorial pixel value multiplied by the myocardial factor).

ples may be due to the transit time of radioactive bolus from the left ventricular cavity to the sampling site in the abdominal aorta. Furthermore, spillover of activity from the blood pool to the myocardial factor was not observed [e.g., lack of an early peak in the myocardial factor (Fig. 3)]. These results demonstrate the capability of FADS in generating pure factors from ^{13}N-dynamic ammonia PET studies.

The assumption that MBF_f is small (e.g. <0.3 ml/min/g) in the derivation of Equation 12 needs to be justified. In the ten dog studies, nine MBF_f (<0.27) satisfied the assumption and one MBF_f equaled 0.48 (study 1). When sectorial MBFs were estimated using the original and adjusted MBF_f in study 1 (0.48 and 0.23 ml/min/g, respectively, the adjusted MBF_f is estimated from half of the myocardial factor as described in Materials and Methods) and compared (the differences were small, <6%). Therefore, sectorial MBF errors would have been small if the unadjusted MBF_f (0.48)

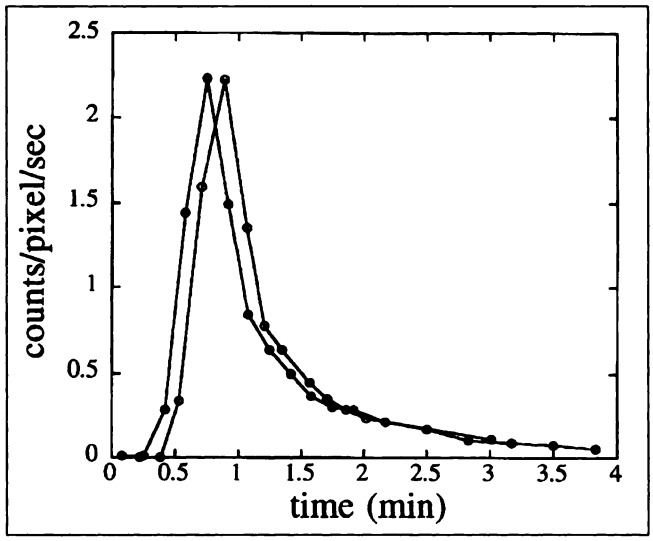

FIGURE 7. Comparison of plasma samples (corrected for nonammonia metabolites) (open circle) and the left ventricular factor (corrected for nonammonia metabolites and scales) (solid circle) from a ^{13}N-ammonia dog PET study. Results were consistent in all ten studies.

was used. Figure 6 showed good correlation between MBFs obtained from the FADS method and conventional two-compartmental model fitting (slope = 1.02, r = 1.0, n = 80). The good correlation (Figure 5A), slope = 0.95, r = 0.96, n = 80) between FADS and the microsphere technique further verifies the use of Equation 12 in converting the myocardial factor image to the parametric MBF image.

Although Patlak graphical analysis (Patlak parametric image generation requires ~10 sec on a SPARC® 10 SUN workstation, Mountain View, CA) is computationally faster than the FADS technique (2 ~ 3 min), FADS-generated parametric MBF images have lower noise levels compared to Patlak parametric images (Fig. 6, rows 2 and 3). When regional MBF calculation is desired, Patlak graphical analysis and conventional modeling methods require TAC generation and linear or nonlinear regression in each region (each nonlinear regression requires ~10 sec). The FADS technique, however, requires only one nonlinear regression of the myocardial factor in the formation of a parametric image; the MBF calculation in any pixel location can then be calculated using Equation 12. The decreased noise in FADS-generated parametric images may be due to removal of spillover activity from the blood pool and reduction of noise when the myocardial factor images were generated. Patlak parametric MBF images in this study were generated by constraining the intercept of the Patlak equation within the physiological range (lower limit: 0.43, upper limit: 0.65) estimated from human studies (*13*). These constraints may not be appropriate for the canine model and may explain the artifacts in some images (e.g., ninth image in row 2 of Fig. 4).

Except for the manually applied mask, all the other steps in this study can be automated (Fig. 1). The computationally time-consuming steps were the axis oblique rotation and nonlinear regression on the myocardial factor. For a three-factor study on the midventricular plane, the procedure required approximately 2 ~ 3 min of computation time. Since we used a command language (MATLAB®) in a SPARC® 10 SUN workstation, the computation time is expected to be shortened by implementing programs using a lower level language such as C. Although three factors were generated using FADS in each study, it might be beneficial if these factors could be applied to additional studies. Due to the variability of the input functions and heterogeneous myocardial uptake among subjects, a separate factor analysis for each study is required.

CONCLUSION

Regional MBF can be measured accurately and noninvasively from ^{13}N-ammonia dynamic PET imaging and the FADS technique. FADS provides a simple method to accurately map the distribution and magnitude of myocardial perfusion and produces parametric MBF images without blood sampling and spillover correction.

ACKNOWLEDGMENTS

The authors thank the UCLA cyclotron staff for synthesizing the ^{13}N-ammonia used in this study, Mr. Ron Sumida and the UCLA PET scanner staff for performing the PET studies; and Drs. E.J. Hoffman, M. Dahlbom, A.R. Ricci, K. Gardner and D. Truong for instrumentation, computer hardware and software support. This work was supported in part by Department of Energy grant DE-SC03-87ER60615 and National Institutes of Health grant NIH-HL29845.

REFERENCES

1. Smith GT, Huang SC, Nienaber CA, Krivokapich J, Schelbert HR. Noninvasive quantification of regional myocardial blood flow with ^{13}N ammonia and dynamic PET [Abstract]. *J Nucl Med* 1988;29:940.
2. Krivokapich J, Smith GT, Huang SC, et al. Nitrogen-13-ammonia myocardial imaging at rest and with exercise in normal volunteers Quantitation of absolute myocardial perfusion with dynamic positron emission tomography. *Circulation* 1989;80:1328–1337.
3. Kuhle WG, Porenta G, Huang SC, et al. Quantification of regional myocardial blood flow using ^{13}N-ammonia and reoriented dynamic positron emission tomographic imaging. *Circulation* 1992;86:1004–1017.
4. Henze E, Huang SC, Ratib O, et al. Measurements of regional tissue and blood-pool radiotracer concentrations from serial tomographic images of the heart. *J Nucl Med* 1983;24:987–996.
5. Wu HM, Hoh CK, Choi Y, et al. Factor analysis for extraction of blood time activity curve in dynamic PET-FDG studies. *J Nucl Med* 1995;36:1714–1722.
6. Barber DC. The use of principal components in the quantitative analysis of gamma camera dynamic studies. *Phys Med Biol* 1980;25:283–292.
7. Cavailloles F, Bazin JP, Di Paola R. Factor analysis in gated cardiac studies. *J Nucl Med* 1984;25:1067–1079.
8. Samal M, Surova H, Karny M, Marikova E, Michalova K, Dienstbier Z. Enhancement of physiological factors in factor analysis of dynamic studies. *Eur J Nucl Med* 1986;12:280–283.
9. Helal BO, Frouin F, Schaison G, et al. Diagnosis of malignancy in thyroid nodules by factor analysis of spectral and dynamic structures: a simultaneous dual-isotope dynamic study with thallium-201 and iodine-131. *Eur J Nucl Med* 1992;19:517–521.
10. Di Paola R, Bazin JP, Aubry F, et al. Handling of dynamic sequences in nuclear medicine. *IEEE Trans Nucl Sci* 1982;NS29:1310–1321.
11. Billotey C, Aurengo A, Najean Y, et al. Identifying abnormal parathyroid glands in the thyroid uptake area using technetium-99m-sestamibi and factor analysis of dynamic structures. *J Nucl Med* 1994;35:1631–1636.
12. Nijran KS, Barber DC. Factor analysis of dynamic function studies using a priori physiological information. *Phys Med Biol* 1986;31:1107–1117.
13. Choi Y, Huang SC, Hawkins RA, et al. A simplified method for quantification of myocardial blood flow using nitrogen-13-ammonia and dynamic PET. *J Nucl Med* 1993;34:488–497.
14. Kuhle WG, Porenta G, Huang SC, Phelps ME, Schelbert HR. Issue in the quantitation of reoriented cardiac PET images. *J Nucl Med* 1992;33:1235–1242.
15. Heymann M, Payne B, Hoffman J, Rudolph A. Blood flow measurements with radionuclide-labeled particles. *Prog Cardiovasc Dis* 1977;20:55–79.
16. Porenta G, Kuhle W, Czernin J, et al. Gated PET imaging permits parameter estimation of cardiac geometry: validation using gated MR imaging and echocardiography [Abstract]. *J Nucl Med* 1991;32:927.
17. Weinberg IN, Huang SC, Hoffman EJ, et al. Validation of PET-acquired input functions for cardiac studies. *J Nucl Med* 1988;29:241–247.
18. Schelbert HR, Phelps ME, Huang SC, et al. Nitrogen-13 ammonia as an indicator of myocardial blood flow. *Circulation* 1981;63:1259–1272.
19. Czernin J, Muller P, Chan S, et al. Influence of age and hemodynamics on myocardial blood flow and flow reserve. *Circulation* 1993;88:62–69.